A fast high-precision six-degree-of-freedom relative position sensor

Gary B. Hughes[a], Van P. Macasaet[b], Janelle Griswold[c], Claudia A. Sison[a], Philip Lubin[c], Peter Meinhold[c], Jonathan Suen[c], Travis Brashears[c], Qicheng Zhang[c], and Jonathan Madajian[c]

gbhughes@calpoly.edu

[a]Statistics Department, California Polytechnic State University, San Luis Obispo, CA

[b]Aerospace Engineering Department, California Polytechnic State University, San Luis Obispo, CA

[c]Physics Department, University of California, Santa Barbara, CA

ABSTRACT

Lasers are commonly used in high-precision measurement and profiling systems. Some laser measurement systems are based on interferometry principles, and others are based on active triangulation, depending on requirements of the application. This paper describes an active triangulation laser measurement system for a specific application wherein the relative position of two fixed, rigid mechanical components is to be measured dynamically with high precision in six degrees of freedom (DOF). Potential applications include optical systems with feedback to control for mechanical vibration, such as target acquisition devices with multiple focal planes. The method uses an array of several laser emitters mounted on one component. The lasers are directed at a reflective surface on the second component. The reflective surface consists of a piecewise-planar pattern such as a pyramid, or more generally a curved reflective surface such as a hyperbolic paraboloid. The reflected spots are sensed at 2-dimensional photodiode arrays on the emitter component. Changes in the relative position of the emitter component and reflective surface will shift the location of the reflected spots within photodiode arrays. Relative motion in any degree of freedom produces independent shifts in the reflected spot locations, allowing full six-DOF relative position determination between the two component positions. Response time of the sensor is limited by the read-out rate of the photodiode arrays. Algorithms are given for position determination with limits on uncertainty and sensitivity, based on laser and spot-sensor characteristics, and assuming regular surfaces. Additional uncertainty analysis is achievable for surface irregularities based on calibration data.

Keywords: laser metrology, dynamic measurement, real-time estimation, in-process metrology, structural metrology

1. INTRODUCTION

1.1. Laser Measurement Systems

The use of optoelectronic methods for dimensional metrology has many advantages, particularly when compared to mechanical methods. Optoelectronic measuring systems can acquire more data in less time and without contacting the measured object. Mechanical measuring systems can be prone to significant errors and deformities due to rapid wear.[1-4] Linear encoders with optical grating scales are the most common optoelectronic measuring devices used for high-precision applications. Simple optical encoder systems are based on the geometrical effect of phase-shifted optical relays for the conversion of the grating displacement relative to the read head into an electrical signal.[5] Linear encoders tend to be robust, even under unstable environmental conditions.

Since the invention of the helium-neon laser, in 1960, lasers have been used as coherent light sources for laser interferometry measurement systems. Optical laser interferometry is often used for displacement measurement applications that require high accuracy. Laser interferometers use a scale length of a well-defined wavelength and link it to the meter by frequency comparison definition. Homodyne sensors use two waves with the same wavelength that are phase shifted by 90 degrees and generated by polarization optics to determine the direction of motion and two additional signals with opposite phase are used to correct changes in the optical intensity. Heterodyne sensors compare slightly different frequencies with a reference bean, allowing the beat frequency of the interference signal to be detected. The phase of the beat frequency changes with the motion of the mirrors and can then be compared with a fixed reference frequency.

Triangulation sensors are often used for in-process metrology and coordinate metrology. Triangulation sensors exploit a collimated light source, generally a laser diode, and a detector unit. The detector unit consists of an imaging lens and a position-sensitive detector[5]. The optical axes of the imaging lens with the light source form a fixed angle. The surface of the object is brought close to the axes point of intersection and the diffused reflection of light is imaged

Photonic Instrumentation Engineering III, edited by Yakov G. Soskind, Craig Olson, Proc. of SPIE Vol. 9754, 975403 · © 2016 SPIE
CCC code: 0277-786X/16/$18 · doi: 10.1117/12.2211372

onto the detector. Typical measurement ranges for triangulation systems are 2 m to 200 mm and can provide relative position measurements with resolutions in the range of 10^{-4} m.

1.2. Dynamic Metrology

Dynamic metrology is concerned with the measurement of quantities that are time-dependent.[6-26] As the characteristics of interest are changing through time, methods of time series analysis have been employed to provide point estimate and uncertainty evolution based on data acquisition through time. Dynamic structural metrology, for instance, is concerned with how the relative position of components in a structure changes through time, as the structure flexes with temperature changes and vibrates in structural modes. Such technology has been developed for atomic force microscopes (AFMs). In an AFM, a molecular tip is mounted on the free end of a cantilever. As the tip is moved across the surface of a sample, molecular-scale movements of the cantilever are induced. A laser is reflected off the back side of the cantilever, and detected at a split photodiode. Movements of the cantilever are detected in the changing position of the laser spot on the photodiode. The AFM cantilever provides a ~3-DOF measurement system (although typical AFM systems only sense one or perhaps two of the potential movements). The AFM tip is typically a flat surface, and the single reflected laser spot moves across the photodiode. In a modification of AFM technology, 6-DOF measurement of the tip position could be attained by using an array of lasers, and by including a curved reflective surface such as a pyramid or hyperbolic paraboloid. The multiple reflected spots would be sensed, and changes in the relative position of the emitter component and reflective surface will shift the location of the reflected spots. Various motions produce independent shifts in the reflected spot locations, allowing full 6-DOF relative position determination. This paper describes an implementation of such a 6-DOF sensor. The sensors are illustrated as part of a system to correct for mechanical flexing of a structure with multiple target acquisition sensors. The sensors are envisioned to make control-time measurements of the relative position of sensor housings within a local mechanical datum coordinate system, thus improving the target vector from the sensing structure.

2. A DYNAMIC RELATIVE POSITION SENSOR CONCEPT

2.1. Sensor Concept

A sensor is envisioned to make dynamic measurements of the relative position of two components. The method uses an array of several laser emitters mounted on one component. The lasers are directed at a reflective surface on the second component. The reflective surface consists of a piecewise-planar pattern such as a pyramid, or more generally a curved reflective surface such as a hyperbolic paraboloid. The reflected spots are sensed at 2-dimensional photodiode arrays on the emitter component. Changes in the relative position of the emitter component and reflective surface will shift the location of the reflected spots within photodiode arrays. Relative motion in any degree of freedom produces independent shifts in the reflected spot locations, allowing full 6-DOF relative position determination between the two component positions. Response time of the sensor is limited by the read-out rate of the photodiode arrays.

In one implementation, consider a series of parallel laser emitters mounted on the first component. Such an arrangement can be thought of as originating from a grid pattern in a fixed ‘emitter plane’ that is normal to the beam vector. A series of photodiode array detectors might be positioned at appropriate places within the emitter plane. Positions of each detector in the emitter plane depend on properties of the reflective surface, which is mounted on the second component. Many implementations are possible; the results presented in this paper are based on parallel emitters, with a suitable pattern of detectors in an emitter plane on the first component. The reflected beam locations in the emitter plane depend on the relative position of the two components. Geometric ray-tracing of the beam paths from the emitter plane (on the first component) to the reflective surface (on the second component) and back to the detectors (on the first component) provides a forward transformation that can predict the detected beam pattern for any relative alignment of the two components. Inversion of the forward transformation can be used to determine the relative alignment of the two components from a specific (measured) beam pattern. Transformations are described below for a 3-panel pyramid reflector, and for a hyperbolic paraboloid.

2.2. Pyramid Reflector

Consider an arrangement with several parallel emitters and their associated detectors, all situated in a single ‘emitter plane’ on the first component. Given a (unit-length) emitter direction vector $E = \langle E_1, E_2, E_3 \rangle$, an implicit emitter plane equation is:

$$E \cdot (x, \mathrm{y}, \mathrm{z}) = d_E \tag{1}$$

The emitters can be represented by points P_i (i = 1, 2, …, n_E = number of emitters) in the emitter plane, *e.g.*:

$$P_i = \left(P_{i_1}, P_{i_2}, P_{i_3}\right), \text{ with } E \cdot P_i = d_E \text{ and } E \equiv \frac{(P_j - P_i) \times (P_k - P_i)}{\|\cdot\|} \tag{2}$$

The notation $\|\cdot\|$ indicates the Euclidean norm of the expression in the numerator, forcing the resulting vector to be unit-length. A beam emanates from the i^{th} emitter at point P_i and follows the direction vector E, so the parametric form for each emitter beam as it leaves the emitter plane is:

$$P_i + t \cdot E, \ t \in \mathbb{R}, \ i = 1 \text{ to } n_E \tag{3}$$

A pyramid reflector is constructed on the second component, consisting of 'panels' that reflect the emitted beams back toward the first component. The 'pyramid' shape will constrain the plane orientations, in particular none of the panels will be parallel, so there will be a single point of intersection representing the 'apex' of the pyramid, $A = \langle A_1, A_2, A_3 \rangle$. Reflector panels have (unit-length) normal vectors R_i and the implicit plane equations are:

$$R_i = \langle R_{i_1}, R_{i_2}, R_{i_3} \rangle, \text{ with } R_i \cdot (x, \mathrm{y}, \mathrm{z}) = R_i \cdot A, \ i = 1 \text{ to } n_E \tag{4}$$

The number of panels in the pyramid does not necessarily need to equal the number of emitters, *e.g.*, two or more emitters could strike the same panel; so, the set $\{R_i\}$ could contain repeated vectors, but a reflective plane must be defined for each emitter. The points Q_i where the i^{th} emitter strikes the i^{th} plane is then found by travelling a distance t_i from the emitter location P_i along the emitter direction vector E:

$$Q_i = P_i + t_i \cdot E \tag{5}$$

The distance t_i can be determined directly, since Q_i lies in the reflector panel plane [27], *i.e.*, from Eq. (4):

$$R_i \cdot Q_i = R_i \cdot A \tag{6}$$

Substitute the expression for Q_i from Eq. (5) into Eq. (6):

$$R_i \cdot (P_i + t_i \cdot E) = R_i \cdot A \tag{7}$$

Distribute the inner product across the sum in Eq. (7) to solve for t_i:

$$t_i = \frac{R_i \cdot (A - P_i)}{R_i \cdot E} \tag{8}$$

The points Q_i are then found by:

$$Q_i = P_i + \left(\frac{R_i \cdot (A - P_i)}{R_i \cdot E}\right) \cdot E \tag{9}$$

Assuming specular reflection, the i^{th} incident beam will be reflected across the panel normal R_i at the point Q_i. The reflected beam will lie in a 'reflection plane' containing the point Q_i. A (unit) vector N_i that is normal to the reflection plane can be determined by the cross product of the incident beam vector E and the panel normal vector R_i:

$$N_i = \langle N_{i_1}, N_{i_2}, N_{i_3} \rangle = \frac{E \times R_i}{\|\cdot\|} \tag{10}$$

The incident angle is between E and R_i (which are both unit length):

$$\theta_i = \operatorname{acos}(E \cdot R_i) \tag{11}$$

The reflected beam emanates from Q_i, at an angle $2\theta_i$ from E around the axis of rotation N_i. A (unit) vector S_i in the direction of the reflected light is determined by rotating the incident beam (unit) vector in the rotation plane, *i.e.*, around the rotation vector N_i, by an angle 2θ [27]:

$$S_i = \frac{M_i \cdot E}{\|\cdot\|} \tag{12}$$

$$M_i = \begin{bmatrix} \cos(2\theta_i) + N_{i_1}^2[1 - \cos(2\theta_i)] & -N_{i_3}\sin(2\theta_i) + N_{i_1}N_{i_2}[1 - \cos(2\theta_i)] & N_{i_2}\sin(2\theta_i) + N_{i_1}N_{i_3}[1 - \cos(2\theta_i)] \\ N_{i_3}\sin(2\theta_i) + N_{i_1}N_{i_2}[1 - \cos(2\theta_i)] & \cos(2\theta_i) + N_{i_2}^2[1 - \cos(2\theta_i)] & -N_{i_1}\sin(2\theta_i) + N_{i_2}N_{i_3}[1 - \cos(2\theta_i)] \\ -N_{i_2}\sin(2\theta_i) + N_{i_1}N_{i_3}[1 - \cos(2\theta_i)] & N_{i_1}\sin(2\theta_i) + N_{i_2}N_{i_3}[1 - \cos(2\theta_i)] & \cos(2\theta_i) + N_{i_3}^2[1 - \cos(2\theta_i)] \end{bmatrix} \tag{13}$$

By the same process shown in Eq. (5) through Eq. (8), the points P_i' where the i^{th} reflected beam strikes the emitter plane are found by travelling a distance t_i' from the incident locations Q_i along the reflected direction vectors S_i. The distances t_i' are:

$$E \cdot P_i' = d_E \ \rightarrow \ E \cdot (Q_i + t_i' \cdot S_i) = d_E \ \rightarrow \ t_i' = \frac{d_E - E \cdot Q_i}{E \cdot S_i} \tag{14}$$

And the points P_i' are then found by:

$$P_i' = Q_i + t_i' \cdot S_i \tag{15}$$

Thus far, geometric ray traces from P_i to P_i' have been established as:

$$P_i' = P_i + \left(\frac{R_i \cdot (A - P_i)}{R_i \cdot E}\right) E + \left(\frac{d_E - E \cdot Q_i}{E \cdot S_i}\right) S_i \tag{16}$$

where S_i is defined in Eq. (12) and Eq. (13). The ray trace assumes that the emitters are all parallel and lie in a plane that is normal to the emitter beams, that the rays are sensed in the same emitter plane, and that the reflection is specular. A simulated reflector based on the pyramid reflector model is shown in Fig. 1.

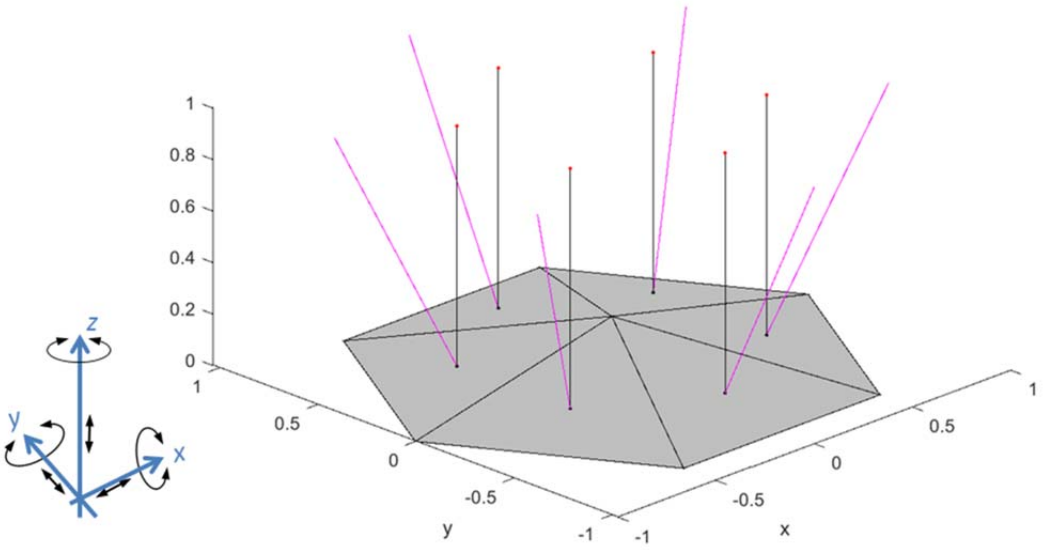

Figure 1. Conceptual diagram of a 6-DOF relative position measurement scheme, using a pyramid reflector. Laser emitters mounted on one component are directed at a reflective pyramid that is mounted on a second component. The reflected spots are sensed in separate 2-D photodiode arrays on the first component. Changes in the relative position of the emitter plane and reflective surface will shift the location of reflected spots. Kinematic and independent motions ensure that the measured spot locations can be used to determine the relative position of the emitter plane and the reflective surface. The implementation in this figure shows six parallel laser emitters emanating from a normal plane, where the detector arrays would also be mounted.

2.3. Hyperbolic Paraboloid Reflector

The same mathematical analysis can be performed for any well-defined reflective surface, *e.g.*, consider a hyperbolic paraboloid. The surface is characterized implicitly as:

$$z = \left(\frac{x}{a}\right)^2 - \left(\frac{y}{b}\right)^2 \quad \rightarrow \quad -\left(\frac{x}{a}\right)^2 + \left(\frac{y}{b}\right)^2 + z = 0 \tag{17}$$

A parametric form is given by:

$$x = a \cdot (u + v) \tag{18a}$$
$$y = b \cdot (u - v) \tag{18b}$$
$$z = 4 \cdot u \cdot v \tag{18c}$$
$$u, v \in \mathbb{R} \tag{18d}$$

Using the parametric form of the emitter beams from Eq. (3), it is possible to find the intersection of the beam and the (parametric) hyperbolic paraboloid, by equating the components with the (parametric) line:

$$P_{i_1} + t \cdot E_1 = a \cdot (u + v) \tag{19a}$$
$$P_{i_2} + t \cdot E_2 = b \cdot (u - v) \tag{19b}$$
$$P_{i_3} + t \cdot E_3 = 4 \cdot u \cdot v \tag{19c}$$

This is not a linear system, since the product of u and v appears in Eq. (19c). However, the system can be solved algebraically, using substitution. Solution of the system yields values t_i, the distances from the emitters P_i to the reflective surface along E:

$$t_i = \frac{4 \cdot u \cdot v - P_{i_3}}{E_3} \tag{20}$$

$$Q_i = P_i + t_i \cdot E \tag{21}$$

The unit vector that is normal to the surface at the point Q_i is N_i:

$$N_i = \frac{\langle \frac{-2Q_{i_1}}{a^2}, \frac{2Q_{i_2}}{b^2}, 1 \rangle}{\|\cdot\|} \tag{22}$$

The remaining steps to determine the geometric ray traces from P_i to P_i' are the same as Eq. (11) through Eq. (16). A simulated reflector based on the hyperbolic paraboloid reflector model is shown in Fig. 2.

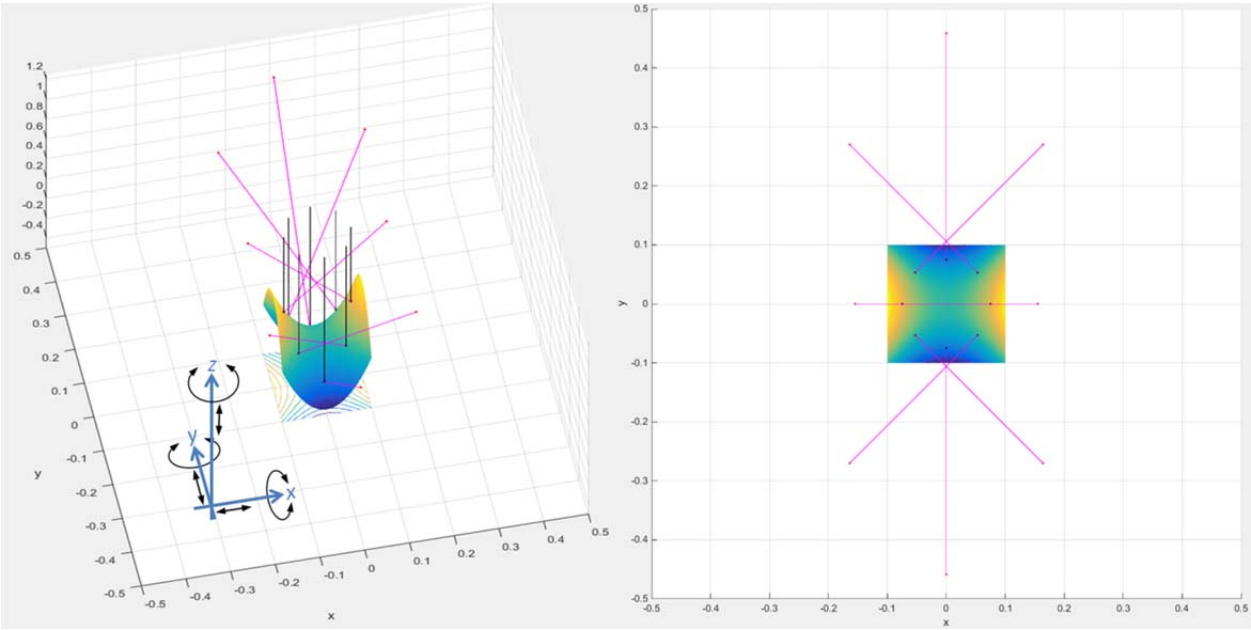

Figure 2. Conceptual diagram of a 6-DOF relative position measurement scheme, using a hyperbolic paraboloid reflector. The implementation in this figure shows six parallel laser emitters emanating from a normal plane, where the detector arrays would also be mounted.

2.4. Relative Position from Reflected Spot Location Measurements

Relative motion of the reflective surface in any of the six degrees of freedom will result in a kinematic displacement of the reflected point P. For example, a translation in the z-axis ($\Delta z \equiv \langle 0, 0, \Delta z \rangle$, which occurs with thermal expansion), results in displacement of P that depends on the distance between the emitter plane and the reflective surface (d), and curvature properties of the reflective surface (determined by a and b):

$$\Delta P = (Q + \Delta z) + \frac{d - E \cdot (Q + \Delta z)}{E \cdot R} \cdot R \tag{23}$$

The change in location of the reflected spot P for a given change in the z-location of the reflective surface is kinematic. For example, for motions in the z-axis, the calculation for change in the reflected spot position is easily invertible:

$$\Delta P = (Q + \Delta z) + \frac{d - E \cdot (Q + \Delta z)}{E \cdot R} \cdot R \quad \rightarrow \quad \Delta z = \frac{(\Delta P - Q)(E \cdot R) - (d - E \cdot Q)R}{E \cdot R - E(3)} \tag{24}$$

Additionally, changes in the reflected multi-spot pattern are independent for motions in the six degrees of freedom when a pyramid, hyperbolic paraboloid or other curved surface is used as the reflecting component. Kinematic motions and independent changes in the spot pattern ensure that position determination is invertible for simultaneous motions in all degrees of freedom, *i.e.*, for some measured change in the spot location from the nominal $\langle \Delta x, \Delta y, \Delta z, \Delta\theta_x, \Delta\theta_y, \Delta\theta_z \rangle$, the relative position of the emitter plane and reflective plane can be determined. The forward ray tracing transformations provide a framework for constrained optimization calculations. Since the number of data points required for the optimization is small, the numerical inversion is fast enough to keep pace with dynamic measurements coming from the photodiodes.

3. A SIMULATED APPLICATION

3.1. Target Acquisition with Multiple Focal Planes

An application of the sensor concept is envisioned as part of a system to correct for mechanical flexing of a structure with multiple target acquisition sensors. The sensors are envisioned to make control-time measurements of the relative position of sensor housings within a local mechanical datum coordinate system, thus improving the target vector from the sensing structure. The target is viewed, for example using an infrared imaging system, consisting of an optic and an infrared focal plane array (IRFPA) that are mounted together in a mechanical housing. A conceptual drawing is shown in Fig. 3, based on a design for an extensible phased array laser system.[28,29]

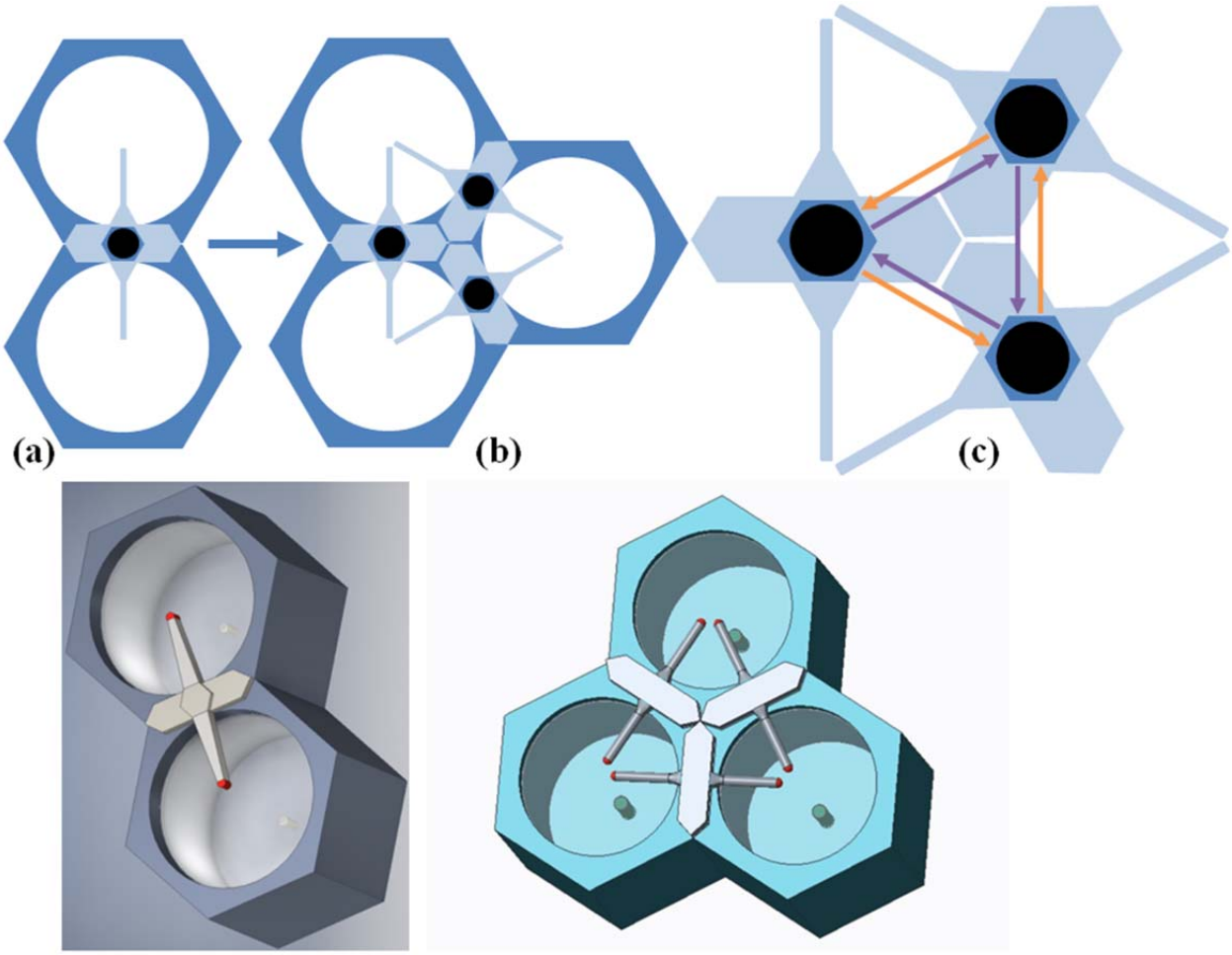

Figure 3. (a) Conceptual diagram of two adjacent cells of a laser phased array; a target sensor is situated between the emitter cells, and phase-tap structures are connected to the sensor housing. **(b)** top view. **(c)** as elements are added to the array, additional target sensors and phase-taps are mounted between adjacent emitters. **(d)** the relative position between adjacent phase tap structures is determined with 6-DOF relative position sensors.

Target acquisition algorithms determine the target centroid $\langle x_c, y_c \rangle$ in the IRFPA pixel array coordinate system. Using camera calibration information, the target centroid $\langle x_c, y_c \rangle$ is then converted to a target axis $\langle \theta_T, \varphi_T \rangle$ as polar (θ) and azimuthal (φ) directions in the infrared camera mount mechanical datum coordinate system, using transformations

deduced from innovative calibration algorithms.[30-33] Conversion from image coordinates to the target axis is accomplished using a composite inverse transformation:[29]

$$\begin{bmatrix}\theta_T\\ \varphi_T\end{bmatrix} = (A\circ D\circ F)^{-1}\left(\begin{bmatrix}x_c\\ y_c\end{bmatrix}\right) \tag{25}$$

where F is the transformation from the target axis to ideal pixel coordinates, D is a lens distortion mapping, and A is the ideal affine transformation from scene coordinates to pixel coordinates, all determined during camera calibration.

The relationship between pixel coordinates and the mechanical mounting is also characterized during fabrication. Precision machining is not adequate for ultra-precision alignment, but statistical calibration/characterization techniques are available. The statistical approach reduces measurement error and supports ultra-precision alignment with 'irregular' machined datum surfaces.

3.2. Pointing and Phase Alignment of a Laser Array

The system depicted in Fig. 3 shows a phased array laser system with multiple target acquisition sensors.[28,29] The relative position of adjacent target sensors is determined using 6-DOF relative position sensors. The emitter plane maintains a rigid spatial relationship within the mechanical datum coordinate system, and the phase tap maintains a rigid spatial relationship to the reflective plane. Using the relative position of the reflective plane, and the rigid relationships, the position of the phase tap within the mechanical datum coordinate system is determined. The target axis $\langle \theta_T, \varphi_T \rangle$ in the mechanical datum coordinate system is used to establish the target plane, which (arbitrarily) passes through the datum origin. The plane becomes the phase reference plane, which is:

$$N_T \cdot \langle x, y, z \rangle = 0, \;\; N_T = \frac{\langle \cos(\theta_T)\sin(\varphi_T), \sin(\theta_T)\sin(\varphi_T), 1 \rangle}{\| \langle \cos(\theta_T)\sin(\varphi_T), \sin(\theta_T)\sin(\varphi_T), 1 \rangle \|} \tag{26}$$

A single phase tap structure connects two adjacent emitters. A nominal location of the phase taps within the mechanical datum coordinate system are determined during factory calibration. The target plane is the phase reference plane: the control system must seek to align the phases of all emitters to the same value at the target plane. Deviations from the calibrated (mechanical datum) location of the phase taps are determined in control time with AFM relative position sensors. The distance of the phase taps from the phase reference plane can then be determined.

$$D_{ref} = \frac{N_T \cdot \langle x_{tap}, y_{tap}, z_{tap} \rangle}{\|N_T\|} = N_T \cdot \langle x_{tap}, y_{tap}, z_{tap} \rangle \tag{27}$$

Distance along the target vector from the phase tap provides the phase alignment target at the phase tap. Phase alignment is modulo one cycle, *e.g.*, shift the measured phase ϕ_{meas} of an emitter to zero in the phase alignment plane:

$$\Delta\phi = \phi_{meas} - \frac{\frac{D_{ref}}{\lambda} - \left\lfloor \frac{D_{ref}}{\lambda} \right\rfloor}{2\pi} \tag{28}$$

4. CONCLUSIONS

A design and method for a fast, 6-DOF relative position sensor are described. The sensor is based on active triangulation laser measurements, and is suitable for applications where the relative position of two fixed, rigid mechanical components is to be measured dynamically with high precision. The method uses an array of several laser emitters mounted on one component, which are directed at a reflective surface on the second component. The reflective surface is curved; examples are described using a pyramid and a hyperbolic paraboloid. The reflected spots are sensed at 2-dimensional photodiode arrays on the emitter component. Changes in the relative position of the emitter component and reflective surface shift the location of the reflected spots within photodiode arrays. Relative motion in any degree of freedom produces independent shifts in the reflected spot locations, allowing full six-DOF relative position determination between the two component positions. Response time of the sensor is limited by the read-out rate of the photodiode arrays. Position is determined using constrained optimization, and can be implemented in FPGA. Limits on relative position uncertainty and sensitivity are achievable, based on laser and spot-sensor characteristics, and assuming regular surfaces. Continuing work will address uncertainty analysis, including deviations due to surface irregularities. The sensor is being developed to support a system with multiple target acquisition sensors. As the sensors must be mounted within a mechanical structure subject to vibration. The sensors are envisioned to make control-time measurements of the relative position of sensor housings within a local mechanical datum coordinate system, thus improving the target vector from the sensing structure.

ACKNOWLEDGEMENTS

We gratefully acknowledge the support and funding from the NASA NIAC 2015 grant NNX15AL91G, and the NASA California Space Grant NASA NNX10AT93H in support of this research.

REFERENCES

[1] Chugui, Y.V. "Three-dimensional optoelectronic measurement systems and laser technologies for scientific and industrial applications," *Optoelectronics, Instrumentation and Data Processing*, 51(4), 385-397 (2015).

[2] Chugui, Y.V., Verkhogliad, A., Kalikin, V., and Zav'yalov, P. "3D optical measuring technologies for industrial applications," *Optical Measurement Systems for Industrial Inspection VII*, edited by Peter H. Lehmann, Wolfgang Osten, Kay Gastinger, Proc. of SPIE Vol. 8082, 808222 (2011).

[3] Chugui, Y.V., Verkhoglyad, A., Poleshchuk, A., Korolkov, V., Sysoev, E., and Zavyalov, P. "3D Optical Measuring Systems and Laser Technologies for Scientific and Industrial Applications," *Measurement Science Review*, *13*(6), 322-328 (2013).

[4] Chugui, Y.V., Bazin, V.S., Finogenov, L.V., Makarov, S.N., and Verkhogliad, A.G. "Optical electronic measuring systems and laser technologies for scientific and industrial applications," *Sixth International Symposium on Instrumentation and Control Technology: Signal Analysis, Measurement Theory, Photo-Electronic technology, and Artificial Intelligence*, edited by Jiancheng Fang, Zhongyu Wang, Proc. of SPIE Vol. 6357, 63571T (2006).

[5] Schwenke, H., Neuschaefer-Rube, U., Pfeifer, T., and Kunzmann, H. "Optical methods for dimensional metrology in production engineering," *CIRP Annals-Manufacturing Technology*, 51(2), 685-699 (2002).

[6] Garcia, E., Hausotte, T., and Amthor, A. "Bayes filter for dynamic coordinate measurements – Accuracy improvement, data fusion and measurement uncertainty evaluation," *Measurement*, 46, 3737–3744 (2013).

[7] Hessling, J.P. "Propagation of dynamic measurement uncertainty," *Measurement Science and Technology*, 22(10), 105105 (2011).

[8] Hessling, J.P. "A novel method of evaluating dynamic measurement uncertainty utilizing digital filters," *Measurement Science and Technology*, 20(5), 055106 (2009).

[9] Hessling, J.P. "Dynamic metrology—an approach to dynamic evaluation of linear time-invariant measurement systems," *Measurement Science and Technology*, 19(8), 084008 (2008).

[10] Hessling, J.P. "A novel method of estimating dynamic measurement errors," *Measurement Science and Technology*, 17, 2740-2750 (2006).

[11] Elster C., and Link A. "Uncertainty evaluation for dynamic measurements modelled by a linear time-invariant system," *Metrologia*, 45, 464-473 (2008).

[12] Vasilevskyi, O. M., Kucheruk, V. Y., and Kurytnik, I. P. "An approach to the evaluation of dynamic uncertainty in measurement using non-statistical techniques," *PAK*, 60(11), 997-1001 (2014).

[13] Vasilevskyi, O. M. "A frequency method for dynamic uncertainty evaluation of measurement during modes of dynamic operation," *International Journal of Metrology and Quality Engineering*, 6(2), 202 (2015).

[14] D'Errico, G.E., and Murru, N. "Real-time estimation of dynamic-multidimensional measurands," *Proceedings of the XX IMEKO World Congress, Metrology for green growth, Busan, Republic of Korea*, (2012).

[15] D'Errico G.E., and Murru, N. "An algorithm for concurrent estimation of time-variant quantities," *Measurement Science and Technology*, 23(4), 045008 (2012).

[16] Beraldin, J.A., Blais, F., Rioux, M., Domey, J., Gonzo, L., De Nisi, F., Comper, F., Stoppa, D., Gottardi, M. and Simoni, A. "Optimized position sensors for flying-spot active triangulation systems," *Proceedings of the Fourth International Conference on 3-D Digital Imaging and Modeling (3DIM)*, NRC 47083, 334-341 (2003).

[17] Beraldin, J. A., and Gaiani, M. "Evaluating the performance of close-range 3D active vision systems for industrial design applications," *Electronic Imaging*, Proceedings of SPIE 5665, 67-77 (2005).

[18] Isheil, A., Gonnet, J.P., Joannic, D., and Fontaine, J.F. "Systematic error correction of a 3D laser scanning measurement device," *Optics and Lasers in Engineering*, 49(1), 16-24 (2011).

[19] English, C., Zhu, S., Smith, C., Ruel, S., and Christie, I. "Tridar: A hybrid sensor for exploiting the complimentary nature of triangulation and LIDAR technologies, *Proceedings of the 8th International Symposium on Artificial Intelligence, Robotics and Automation in Space*, ESA SP-603 (2005).

[20] English, C., Okouneva, G., Saint-Cyr, P., Choudhuri, A., and Luu, T. "Real-time dynamic pose estimation systems in space: lessons learned for system design and performance evaluation," *International Journal of Intelligent Control and Systems*, 16(2), 79-96 (2011).

[21] Deb, S., Yeddanapudi, M., Pattipati, K., and Bar-Shalom, Y. "A generalized SD assignment algorithm for multisensor-multitarget state estimation," *IEEE Transactions on Aerospace and Electronic Systems*, 33(2), 523-538 (1997).

[22] Weckenmann, A., Jiang, X., Sommer, K.D., Neuschaefer-Rube, U., Seewig, J., Shaw, L., and Estler, T. "Multisensor data fusion in dimensional metrology," *CIRP Annals-Manufacturing Technology*, *58*(2), 701-721 (2009).

[23] Sun, S.L., and Deng, Z.L. "Multi-sensor optimal information fusion Kalman filter," *Automatica*, 40(6), 1017-1023 (2004).

[24] Sun, S.L. "Multi-sensor optimal information fusion Kalman filters with applications," *Aerospace Science and Technology*, 8(1), 57-62 (2004).

[25] Xiong, N., and Svensson, P. "Multi-sensor management for information fusion: issues and approaches," *Information fusion*, 3(2), 163-186 (2002).

[26] Khaleghi, B., Khamis, A., Karray, F.O., and Razavi, S.N. "Multisensor data fusion: A review of the state-of-the-art," *Information Fusion*, 14(1), 28-44 (2013).

[27] Hughes, G.B. "Algorithms for sensor chip alignment to blind datums," *Journal of Electronic Imaging*, 15(3), 033003 (2006).

[28] Lubin, P., Hughes, G.B., Bible, J., Bublitz, J., Arriola, J., Motta, C., Suen, J., Johansson, I., Riley, J., Sarvian, N., Clayton-Warwick, D., Wu, J., Milich, A., Oleson, M., Pryor, M., Krogen, P., Kangas, M., and O'Neill, H. "Toward directed energy planetary defense," *Optical Engineering*, 53(2), 025103 (2014).

[29] Steffanic, P., Johannes, B.T., Sison, C.A., Hughes, G.B., Lubin, P., Meinhold, P., Suen, J., O'Neill, H., Kangas, M., Brashears, T., Zhang, Q., Griswold, J., Riley, J., and Motta, C. "Local phase control for a planar array of fiber laser amplifiers," *Nanophotonics and Macrophotonics for Space Environments IX*, edited by Edward W. Taylor, David A. Cardimona, *Proc. of SPIE*, 9616 (2015).

[30] Tsai, R.Y. "A versatile camera calibration technique for 3D machine vision metrology using off-the-shelf TV cameras and lenses," *IEEE Journal of Robotics & Automation*, RA-3(4), 323-344 (1987).

[31] Zhang, Z. "A flexible new technique for camera calibration," *IEEE Transactions on Pattern Analysis and Machine Intelligence*, 22(11), 1330-1334 (2000).

[32] Sun, Q., Hou, Y., Tan, Q., and Li, G. "A flexible calibration method using the planar target with a square pattern for line structured light vision system," *PLOS One*, 9(9), e106911 (2014).

[33] Kannala, J., and Brandt, S.S. "A generic camera model and calibration method for conventional, wide-angle, and fish-eye lenses," *IEEE Transactions on Pattern Analysis and Machine Intelligence*, 28(8), 1335-1340 (2006).